Citation: BoneKEy Reports **5**, Article number: 829 (2016) | doi:10.1038/bonekey.2016.60
© 2016 International Bone & Mineral Society All rights reserved 2047-6396/16
www.nature.com/bonekey

REVIEW

Post-yield and failure properties of cortical bone

Uwe Wolfram[1] and Jakob Schwiedrzik[2]

[1]School of Engineering and Physical Science, Institute for Mechanical, Process and Energy Engineering, Heriot-Watt University, Edinburgh, UK. [2]Empa, Swiss Federal Laboratories for Materials Science and Technology, Laboratory for Mechanics of Materials and Nanostructures, Thun, Switzerland.

Ageing and associated skeletal diseases pose a significant challenge for health care systems worldwide. Age-related fractures have a serious impact on personal, social and economic wellbeing. A significant proportion of physiological loading is carried by the cortical shell. Its role in the fracture resistance and strength of whole bones in the ageing skeleton is of utmost importance. Even though a large body of knowledge has been accumulated on this topic on the macroscale, the underlying micromechanical material behaviour and the scale transition of bone's mechanical properties are yet to be uncovered. Therefore, this review aims at providing an overview of the state-of-the-art of the post-yield and failure properties of cortical bone at the extracellular matrix and the tissue level.

BoneKEy Reports **5**, Article number: 829 (2016) | doi:10.1038/bonekey.2016.60

Introduction

Skeletal diseases such as osteoporosis constitute serious personal, social and economic burdens. Osteoporosis affects 200 million women and causes 9 million fractures annually worldwide. Hip fracture incidence alone is projected to increase 240% in women and 310% in men by 2050. At the same time Europe will face associated costs of approximately €77 billion per year while in China over 500 million inhabitants are expected to suffer from osteoporosis see, for example, http://www.iofbonehealth.org/facts-statistics (last accessed on 01/02/2016) for more information.

Age-related fractures lead to a loss of mobility, an increased mortality and a lower quality of life in general. A significant proportion of physiological loading is carried by the cortical shell.[1,2] Thus, its role in the fracture resistance and strength of whole bones is important.[3–5] Whole-bone strength has been shown to depend on the tissue mineralisation measured by clinical densitometry, but also on the micromechanical properties of the hierarchical organisation of bone tissue.[6,7] Therefore, this paper aims at reviewing the post-yield and failure properties of cortical bone at the extracellular matrix (ECM) and the tissue level.

Defining Post-Yield Behaviour and Some Nomenclature

The mechanical behaviour of cortical bone (**Figure 1**) can be characterised by (i) an initial elastic domain where the material deforms in a reversible fashion, (ii) a post-yield domain where irreversible strains and damage are produced and (iii) a fracture zone where a macrocrack is formed. These domains can be more or less pronounced, as for instance in tension, the formation of a macrocrack is a rapid event once the ultimate point is passed. Altogether the zones represent an area that is equal to the mechanical work necessary to break the specimen. Zone I represents the elastic mechanical work and the sum of zone II and III yield the plastic mechanical work, see for example, Lemaitre and Chaboche.[8]

The elastic domain I is limited by a yield point, which represents a threshold from where irreversible deformation is accumulated. This point is an alternative representation of a critical strain energy and may be represented as a function of the six independent components of the stress or strain tensor.[9] Unlike in steel, where the yield point can be relatively clearly distinguished, yielding in bone is rather associated with a continuous transition zone (**Figure 1**). Several methods are used to approximate this point, such as, an offset-criterion where the intercept of the stress–strain curve with a line with a slope equal to the initial stiffness E_0 and shifted by a strain-offset is evaluated. An offset of 0.2%[10] can include considerable non-linearity whereas 0.05%[11] seems to provide a better approximation of the start of the non-linear part of the stress–strain curve. Bone can be considered as a quasi-brittle material at the tissue level since many microcracks are developed prior to failure that do not immediately lead to catastrophic failure.[12] Therefore, a critical damage (D^c) criterion[10] may be usable with a chosen, small D^c of, for example, 2.5%. Yield is determined as the intercept of the stress–strain curve with a line passing through zero and with a slope of $(1 - D^c)E_0$. Finally, a critical energy criterion may be used where the area of domain I, elastic work, is evaluated and compared to a critical value.

Correspondence: Dr U Wolfram, School of Engineering and Physical Science, Heriot-Watt University, Institute for Mechanical, Process and Energy Engineering, James Nasmyth Building, Room JN 2.33, Edinburgh EH14 4AS, UK.
E-mail: u.wolfram@hw.ac.uk

Received 9 March 2016; accepted 5 July 2016; published online 24 August 2016

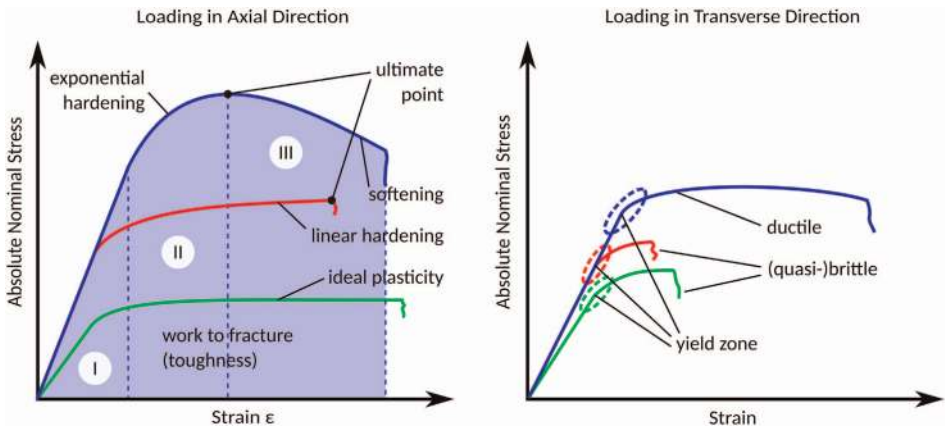

Figure 1 Typical monotonic stress-strain curves are sketched to illustrate the behaviour for tension (red), compression (blue), and shear (green) in axial and transverse loading. The three domains of the mechanical behaviour are an elastic domain I, post-yield or damaging zone II, and a fracture zone III where a macrocrack forms. The form of the curves is deduced from the sources displayed in **Table 1**. Hardening, be it linear or exponential, describes an increase in stress after passing the yield point. Softening, in turn, is a decrease in stress usually observed after passing an ultimate value that may coincide with the yield point. Ideal plasticity denotes an asymptotic behaviour after reaching yield. Brittle, quasi-brittle, and ductile are phenomenological descriptions whether the area underneath the stress-strain curve, i.e. the energy, after passing the yield zone, i.e. region II plus III, is small or large, respectively. Ductility refers to a material's ability to dissipate a lot of mechanical work and it is the opposite of brittleness.

The post-yield domain II is, towards higher strains, delimited by the ultimate point. Unlike yield, this point can be exactly determined from a stress-strain experiment.

The fracture domain III following the ultimate point is out of scope of this review. The load bearing capacity is drastically reduced by formation of a macrocrack after passing the ultimate point. This crack travels through the thickness of the cortical shell and eventually leads to fracture. To investigate this behaviour requires fracture mechanics approaches as used by many authors and we provide a mere starting-point.[13–15]

Cortical Bone Tissue

Bone is a hierarchically structured bio-composite consisting of a cell-seeded mineralised collagen matrix (**Figure 2**). It is mainly composed of mineral (50–60 wt.%), type I collagen (30–40 wt.%), and water (10–20 wt.%).[16] Fibrils consisting of self-assembled collagen molecules are reinforced periodically by mineral platelets in a collagen guided biochemical process.[17–19] Water and noncollagenous proteins fill inter-fibrillar pore space. Of these non-collagenous proteins, osteocalcin strongly binds to minerals while it complexes and links to collagen via osteopontin[20] to help to impregnate the mineralised collagen fibrils by extra-fibrillar mineral particles[13,19] and combine them into fibril arrays making up a mineralised collagen fibre. Assemblies of mineralised collagen fibres form lamellae in a rotated plywood pattern.[21,22] The lacuno-canalicular network provides a habitat for osteocytes and their processes at this length-scale constituting about 1% of bone porosity.[23]

Cortical bone encloses trabecular bone in, for instance, vertebrae or the epiphyses of long bones. It consists of concentric bone lamellae arranged around blood vessels forming osteons and interstitial areas.[24] It features a macroporosity of around 5–15%, which is mainly oriented along the osteon direction.[13] A continuous remodelling process that counteracts the development of fatigue damage results in secondary osteons.[13] Osteons are separated from the surrounding tissue by a cementous interface,[25] which is 1–5 μm in thickness.[13,25] Its exact nature and mechanical role has been widely debated and for instance associated with an increase in toughness, a decrease in strength, a role as crack-arrestor, and an increase in crack-path.[26–30]

Major Determinants of Strength

Cortical bone strength on the organ level has been the subject of a considerable amount of research and **Table 1** provides an overview over yield strain, ultimate strain, yield stress, strength values and the observed hardening behaviour for human cortical bone.

Osteonal porosity is the major determinant of bone strength[13,31–35] despite the importance of other variables such as mineralisation and collagen fibre orientation.[36–38] Although the orientation of the collagen fibres affects its local anisotropic properties, the mineralisation in human bone is relatively constant.[36,32]

A negative correlation was found between porosity and strength,[32,13] which showed a faster decrease of strength in compression compared with tension and torsion.[35] This fast decrease may have been caused by the load case. Tensile and torsional samples remain aligned with the loading axis during testing. For compressive loading, macroscopic samples may become unstable after reaching yield. Microcrack appearance may be accompanied by pore driven deformation localisation and a change from a homogeneous stress state over the cross-section into a state of plastic buckling which can then lead to a decreased strength. This process may be amplified by a higher porosity, as it can act as a stress concentrator and decreases the lateral support of locally buckling regions.

Yield strain in tension and compression, however, is independent of porosity (see citations on strength) and a ratio between yield strain in tension and compression of 0.68 was identified,[35] which is very similar to the ratio of yield strains numerically determined for trabecular bone at the ECM level.[39] Torsional yield strains are significantly dependent on porosity[35] which may be due to the interplay of loading condition and sample geometry.[27] A higher porosity could imply more sectioned osteons at the circumferential surface of the sample. This leads to the presence of weak interfaces and pre-existing

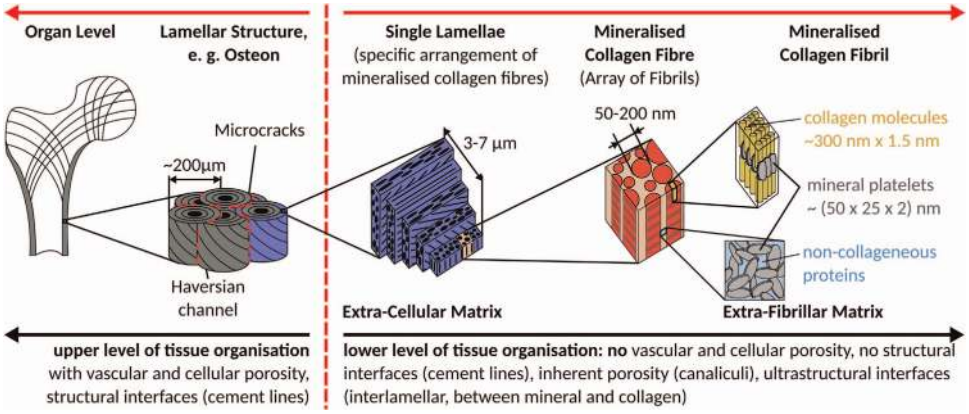

Figure 2 Hierarchical structure of cortical bone tissue. The red dashed line separates the upper level of tissue organisation (macroscopic, organ or tissue level) from the lower level of tissue organisation (microscopic, extracellular matrix level). The image is adopted from Reisinger *et al.*[138]

surface cracks in the most stressed area, which might lead to a decrease of apparent yield strains compared to a pristine sample.

Porosity is indeed the major significant but often weak determinant of macroscopic tensile, compressive and torsional strength.[35] The authors related multiple macro- and micro-mechanical tests, computed tomography, histomorphometry and Raman spectroscopy to each other in order to find the relevant factors determining macroscopic strength. Not included in the study were pre-existing microdamage, bound water and collagen cross-links. The latter two, however, should have influenced the microindentation properties obtained for each sample. As this was not the case, it was concluded that another structural feature such as pre-existing microdamage has a decisive role in the post-yield and failure properties of cortical bone which is in line with observations on the scale transition of mechanical properties, which will be discussed later in this review.[40]

Microdamage

Pre-existing and pre-failure microdamage (**Figure 3**) is not detectable using clinical imaging modalities but is deemed to be the most detrimental factor in defining bone's strength and toughness.[35] Microdamage accumulates due to isolated, non-physiological overloading events in a quasi-static mode or after suffering fatigue from a large number of physiological loading cycles[11,41] and decreases bone's stiffness, strength and toughness.[14,42]

Microdamage can be differentiated into microcracks and diffuse damage which are smaller cracks on a lower length scale.[43] Microcracks appear linear and spatially organised in 2D histological sections with a pertinent length of tens of micrometer.[43–45] In 3D, microcracks are approximately elliptical with an aspect ratio of 4:1 to 5:1.[46] Their thickness is one to two orders of magnitude smaller than their length. Microcracks are associated and guided by microstructural and ultrastructural features of bone.[16,27,47,48] They appear at highly mineralised zones in bone tissue, between interstitial lamellae, along osteonal cement lines, at the boundaries of trabecular packages, at resorption cavities in trabecular bone, and, in case of sub-lamellar microcracking, along the canaliculi in cortical bone.[27,43,47–49]

Microdamage (**Figure 3**) is loading mode dependent[11] as it appears to be different in bone regions loaded primarily in tension compared to regions loaded in compression.[44,50–52] In histology studies, tensile microdamage appears to consist mostly of diffuse cracks oriented normally to the loading axis while compressive microdamage is expressed as cross-hatched microcracks.[44,43,51] This may be due to different yielding processes for tension and compression.[13,53] These processes eventually lead to fracture planes oriented normal to the loading direction in tension and oblique in compression as observed in creep failure experiments.[54] The angle of the cross-hatches (**Figure 3**) was found to be different from 45° in specimens tested in axial, transverse or oblique directions[29] highlighting the impact of the structural anisotropy.

Loading Mode Dependence and Anisotropy

The combination of bone's structural anisotropy and the loading mode dependent and anisotropic nature of microdamage yields loading mode dependent and anisotropic post-elastic behaviour of cortical bone.[11,13,53,55–57] After an initial exponential hardening regime, the monotonic postyield behaviour is characterised by linear hardening in tension, quasi-brittle softening in compression, and ideal plasticity without hardening under shear (**Figure 1**). Hardening in cortical bone is generated by mineralised collagen fibres bridging emerging cracks. It was suggested that bone is plastically compressible[40,58] which might as well contribute to initial hardening under compression next to friction. Softening in compression is dominated by the occurrence of microdamage. Emerging cracks reduce the load carrying cross-section and, with it, the load bearing capacity. In a material that contains many microcracks, two stresses can be defined.[12] The effective stress $\tilde{\sigma}$, is the average stress transmitted by the yet unbroken, that is, effective, area $\tilde{A}$. The total stress σ is the stress acting on the total area A of, for example, a macroscopic test specimen. Both are related by $\sigma = (1-D)\tilde{\sigma}$ where the damage variable $D = \frac{A-\tilde{A}}{A}$ represents the accumulated microcracks. For ideal or asymptotic hardening behaviour, $\tilde{\sigma}$ would be constant or increasing, while σ, and therefore, the load bearing capacity would decrease due to the increasing damage.[12] Ideal plasticity observed in torsion[35] may be dominated by cleavage opening

Table 1 Macroscopic strength values for human cortical bone

Source	d	n	*Age Range in years*	*Test condition*	*Test direction*	*Loading mode*	ε^y *in %*	σ^y *in MPa*	ε^u *in %*	σ^u *in MPa*	*Post-yield behaviour*
Bayraktar *et al.*[33]	34	74	54–85	w	ax	ut	0.73 ± 0.05	107.9 ± 12.3	—	—	ha
Carter *et al.*[127]	4	10	51–84	w	ax	ut	0.84 ± 0.05	121.0 ± 11.0	1.6 ± 0.38	140.0 ± 12.0	ha
Cezayirlioglu *et al.*[60]	4	50	40–80	w	ax	ut	—	121.7 ± 10.2*	3.6 ± 0.83*	145.2 ± 8.4*	ha
		28		w	ax	uc	—	176.3 ± 13.1*	2.8 ± 0.64*	204.0 ± 11.2*	—
		29		w	ax	tr	—	52.5 ± 6.3*	3.0 ± 0.71*	69.0 ± 5.5*	so
Courtney *et al.*[119]	10	28	72 ± 6	w	ax	ut	0.36 ± 0.039	49.3 ± 5.5	—	—	ha
foo	8	28	26 ± 5	w	ax	ut	0.38 ± 0.041	55.3 ± 8.6	—	—	ha
Currey[128]	11	—	3–5	w	ax	ut	0.95	87.45	3.9	134.1	ha
foo	4	—	35	w	ax	ut	0.72	122.3	2.2	165.9	ha
Dickenson *et al.*[129]	11	29	67–87	w	ax	ut	—	80.8 ± 13.7	—	117.0 ± 17.3	ha
Dong *et al.*[62]	8	8	51.5 ± 3.3	w	ax	uc	0.91 ± 0.09	111.0 ± 18.6	—	124.0 ± 15.0	so
		8		w	ci	uc	0.83 ± 0.42	41.8 ± 19.4	—	65.2 ± 13.8	nh
		8		w	ra	uc	0.84 ± 0.23	44.1 ± 21.1	—	63.1 ± 20.7	nh
Dong *et al.*[130]	6	6	76–88	w	ax	sh	0.88 ± 0.18	35.7 ± 9.9	—	61.4 ± 6.3	nh
Duchemin *et al.*[131]	13	46	54–101	w	ax	ut	—	—	—	53.8 ± 20.3	—
		46		w	ax	uc	—	—	—	106.4 ± 29.4	—
Ebacher *et al.*[29]	3	7	55–69	w	ax	uc	1.07 ± 0.14	141.0 ± 5.0	1.3 ± 0.20	143.0 ± 6.0	so
		7		w	tr	uc	1.15 ± 0.07	79.0 ± 7.0	3.3 ± 0.80	91.0 ± 9.0	nh
		3		w	45°	uc	0.98 ± 0.08	104.0 ± 10.0	1.7 ± 0.40	113.0 ± 11.0	so
Evans *et al.*[31]	17	207	36–75	e	ax	ut	—	—	1.5	88.3	ha
Jepsen *et al.*[50]	6	18	25–49	w	ax	tr	1.30 ± 0.10	55.8 ± 3.8	5.2 ± 0.90	74.1 ± 3.2	so
Lee *et al.*[132]	26	11	53–98	w	ax	ut	0.56 ± 0.07	70.6 ± 31.6	2.0 ± 0.85	77.0 ± 42.2	ha
Leng *et al.*[133]	16	16	51–90	w	ax	uc	0.77 ± 0.03	112.5 ± 9.5	—	127.0 ± 8.6	so
Mirzaali *et al.*[35]	39	32	46–99	w	ax	ut	0.45 ± 0.05	71.6 ± 10.2	1.9 ± 0.60	93.0 ± 10.1	ha
		32		w	ax	uc	0.66 ± 0.09	115.1 ± 16.4	1.3 ± 0.30	153.6 ± 21.6	so
		32		w	ax	tr	0.57 ± 0.03	31.6 ± 4.0	—	46.3 ± 5.8	nh
Nyman *et al.*[134]	17	17	51–90	w	ax	ut	0.41 ± 0.02	—	—	100.9 ± 7.3	ha
Reilly *et al.*[55]	19	101	20–86	w	ax	ut	—	—	2.74 ± 0.57	128.3 ± 12.3	ha
		95		w	ax	uc	—	—	2.11 ± 0.33	190.4 ± 15.6	so
Reilly and Burstein[53]	4	21	23–63	w	ax	ut	—	114.0 ± 3.1	3.10 ± 0.72	135.0 ± 15.6	ha
		20		w	tr	ut	—	—	0.70 ± 0.14	53.0 ± 10.7	—
	4	16	21–52	w	ax	uc	—	—	1.87 ± 0.29*	202.3 ± 17.3	so
		12		w	tr	uc	—	—	4.33 ± 1.25*	160.0 ± 20.7	ha
	2	12	23–56	w	ax	tr	—	—	—	68.0 ± 2.9*	—
Saha[135]	14	24	—	e	ax	sh	—	—	—	46.6 ± 9.7*	so
Tang *et al.*[63]	8	10	62–79	w	ax	sh	—	—	—	28.9 ± 6.2	nh
		9		w	30°	sh	—	—	—	31.2 ± 8.4	qb
		5		w	60°	sh	—	—	—	22.7 ± 2.5	qb
		5		w	tr	sh	—	—	—	49.9 ± 6.2	qb
Turner *et al.*[61]	5	11	63–83	w	ax	sh	—	—	—	51.6 ± 1.9	—
		14		w	tr	sh	—	—	—	65.3 ± 2.5	—
Wang and Nyman[136]	9	9	49–59	w	ax	ut	—	—	—	88.1 ± 11.4	ha
	9	9	69–87	w	ax	ut	—	—	—	75.6 ± 13.0	ha
Yamada[137]	60	—	10–19	w	ax	ut	—	—	1.48	113.8 ± 1.5	ha
		—	20–79	w	ax	ut	—	—	1.30 ± 0.014	103.3 ± 2.0*	ha
	33	—	20–59	w	ax	uc	—	—	1.83 ± 0.04	156.9 ± 3.7*	ha
	21	—	20–89	w	ax	tr	—	—	2.67 ± 0.09	52.2 ± 1.0*	ha

Abbreviations: ax, axial in osteonal direction; ci, circumferential; d, number of donors; e, embalmed; n, number of specimens; ob, oblique 45°; ra, radial in a cylindrical coordinate system; sh, shear; tr, transverse to osteonal direction; uc, uniaxial compression; ut, uniaxial tension; w, wet.
Mechanical variables included are, yield strain (ε^y), yield stress (σ^y), ultimate strain (ε^u), and ultimate stress (σ^u). Characteristics of the post yield behaviour (**Figure 1**) are, brittle (br), quasi-brittle (qb), plastic (pl), hardening (ha), ideal plasticity or no hardening (nh). Please note that the tremendous body of work on other species that can be found, for instance, in Currey[12] is not included.
#Given standard deviation $\bar{\sigma}$ are pooled variations for a sample with m means ± standard deviations. σ_m, i.e., $\bar{\sigma} = \sqrt{\sigma_1^2 + \cdots + \sigma_m^2}$.

of the osteonal microstructure while in axial direction friction without fibre bridging may explain the asymptotic post yield behaviour. In transverse loading, the absence of hardening[29] may be due to the formation of a slip-plane parallel to the osteons reinforcing the structure. Such reinforcing elements may also be inactive in transverse tension where the cementous interface could naturally open without the support of bridging fibres which leads to rapid formation of a macrocrack.

The monotonic post-yield behaviour is influenced differently by pre-existing microdamage. Repetitive loading experiments[11] showed that a previous compressive overload deteriorates the tensile elastic and post-elastic properties,

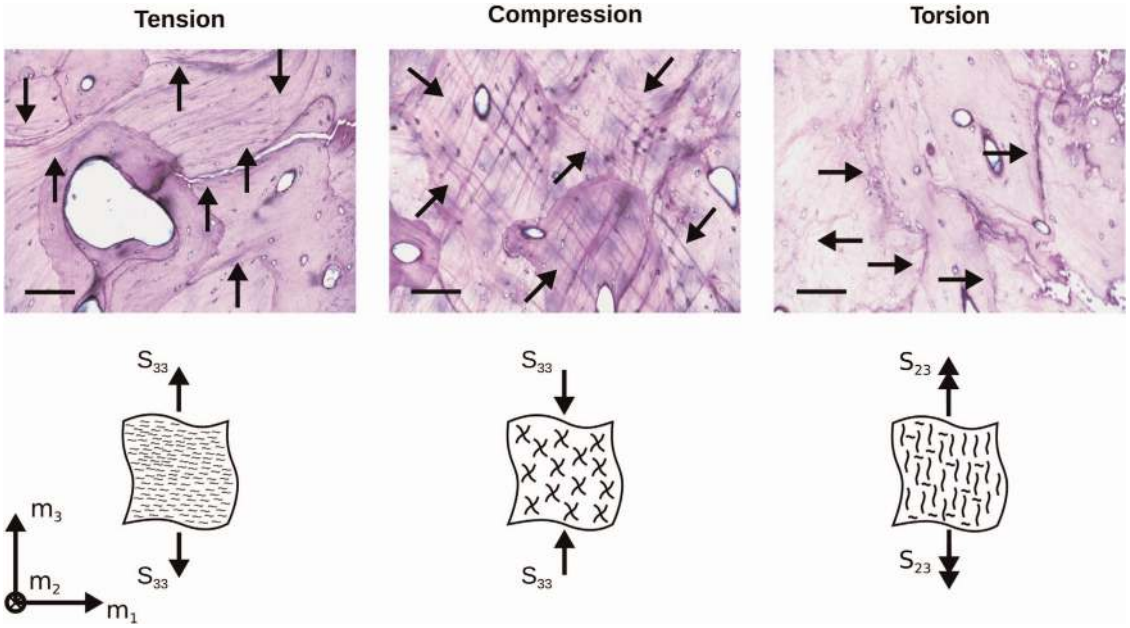

Figure 3 Basic Fuchsin stained, sagittal histological sections of three osteonal samples overloaded in uniaxial tension, uniaxial compression, and torsion are shown.[11] The osteonal main axis is equal to $\mathbf{m}_3$ and the scale bar is 100 μm. Three distinct, loading mode dependent microcrack families can be distinguished as indicated in the sketches. The cracks under tension are smaller and more diffuse than the cross-hatches found under compression or cracks under torsion. Note, that the tensile image was taken close to the final macrocrack of which some effects are partially visible and that small or perpendicular microcracks may close upon unloading[59] and are, thus, difficult to detect histologically.

while a previous tensile overload had only a minor effect on a subsequent compressive load (**Figure 4**). In fact, a previous compressive overload was not only detectable as damage on the compressive side but also reduced tensile yield and strength properties which was not the case *vice versa*. This is in line with crack closure observations upon unloading.[59] This implies that pre-existing compressive microdamage significantly decreases the load bearing capacity in a sideways fall which is tension dominated.

When loaded in transverse direction, the mechanical response changes to a brittle behaviour in tension with hardly any ductile deformation and to an ideal plasticity with no or little hardening and softening in compression (**Figure 1**). Strength is lower (**Tables 1 and 2**) that indicates anisotropic material behaviour. Cortical bone seems to be well described by transverse isotropy, which is most likely due to its osteonal micro-structure.[13,29,53,57,60–63]

In shear, a quasi-brittle behaviour with a lower ductility than in torsion experiments is encountered with slightly increased strength values. Since it was found that osteonal bone is anisotropic under shear,[61,63] it is yet to be confirmed whether only one loading axis is distinct or all three. Transverse isotropy might hold given the osteonal structure and the observation that cement line motion is the major deformation mechanism,[64] which fits well with the observed microdamage (**Figure 3**).

All these values are affected by increasing loading rates which lead to an increase in brittleness and a decrease in strength in tension with hardly an effect on torsional loads.[65–68] Whether this is true for the transverse directions is yet to be confirmed. In addition, changing water content has a significant influence on the mechanical properties.[69] Drying increases strength and decreases ductility and, if similar to the micro-scale,[70] changes anisotropy.

Micromechanical Properties

As bone is a hierarchical composite material, its strength depends greatly on the length scale under observation (**Table 2**). Its properties on the nano- and microscale have a decisive effect on its macroscopic properties and are a major determinant of what is often referred to as 'bone quality', that is, factors despite bone mass influencing fracture risk.

The mechanism by which bone deforms following overloading on the nanoscale has been widely debated. Synchrotron radiation diffraction experiments performed *in situ* on macroscopic tensile specimens showed that the nanometer sized mineral platelets carry a large portion of the load and appear to be flaw insensitive due to their small size, which prevents brittle failure and increases their strength significantly compared to bulk hydroxyapatite.[71] The organic matrix on the other hand is crucial for transferring the load to the mineral platelets. The onset of apparent yielding in parallel fibred bone corresponded to yielding on the fibrillar level: the extrafibrillar matrix starts to flow, which leads to a constant fibrillar elongation at rising apparent strain levels.[72,73] Moreover, after unloading the fibril was at a negative strain value relative to the original configuration. Gupta *et al.*[73] interpreted this as internal decohesion between the mineral platelets and the tropocollagen molecule, which might be interpreted as a damage mechanism. Further experiments at variable temperature and strain rate interpreting the changes in yield stress by an *Arrhenius*-type rate equation showed that the activation energy and volume[74] of the nanoscale deformation mechanism lie in the range of 1 eV and 1 nm^3, respectively.[75] This activation energy is much larger than a hydrogen bond, but considerably smaller than a covalent bond and it most likely corresponds to charge interactions between molecules in the extrafibrillar matrix.[75]

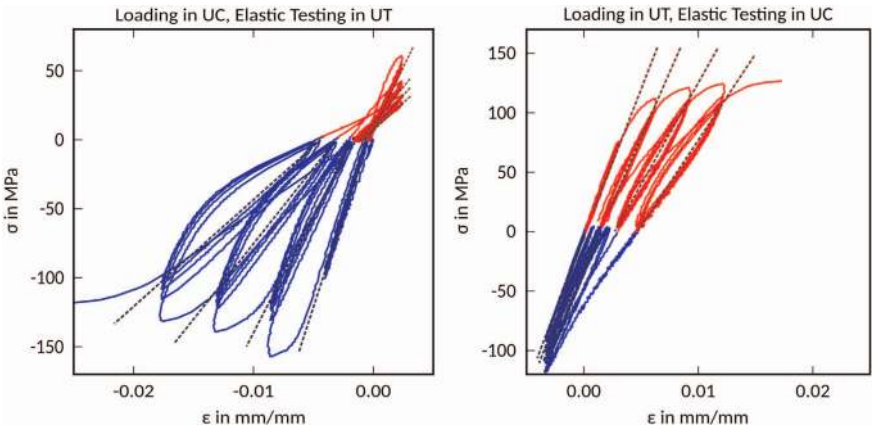

Figure 4 Two example curves from a repetitive loading experiment.[11] Left, overloading in compression (blue) and elastic reloading in tension (red). Right, the same exercise *vice versa*. The dashed lines illustrate how stiffness was identified. The greater effect of a compressive overload on a tensile reload in comparison to a tensile overload and a compressive reload is clearly visible.

Table 2 Microscopic strength values

Source	n	*Species*	*Test condition*	*Test direction*	*Loading mode*	ε^y *in %*	σ^y *in MPa*	ε^u *in %*	σ^u *in MPa*	*Post-yield behaviour*
Schwiedrzik *et al.*[40]	19	ov	v	ax	uc	—	490.0 ± 100.0	—	750.0 ± 60.0	pl
	20	ov	v	tr	uc	—	300.0 ± 20.0	—	590.0 ± 40.0	pl, ha
Luczynski *et al.*[102]	9	bo	v/a	ax	uc	—	—	3.74 ± 0.77	505.1 ± 87.5	pl
Jimenez-Palomar *et al.*[105]	6	ra	v	ax	be	—	—	—	632.0 – 1083.0	br

Abbreviations: a, in air; ax, axial in osteonal direction; bo, bovine; ov, ovine; ra, rat; tr, transverse to osteonal direction; v, in vacuum.
Loading modes are, uniaxial compression (uc) and bending (be). Included variables are yield strain (ε^y), yield stress (σ^y), ultimate strain (ε^u), ultimate stress (σ^u). Characteristics of the post yield behaviour (**Figure 1**) are, brittle (br), plastic (pl), hardening (ha).

Fantner *et al.*[76] reported on the importance of 'sacrificial bonds' and 'hidden lengths' for bone toughness. Sacrificial bonds are weak, re-formable bonds increasing the energy required to stretch molecules to their full length and break them. When sacrificial bonds inside a network break, they allow further unfolding of the molecular structure referred to as 'hidden length'. After removal of strain from the network, the sacrificial bonds can reform, which provides a possible mechanism for repeated dissipation of strain energy.[76,77] Using an atomic force microscopy (AFM) based technique, traction–separation curves of mineralised fibrils were recorded and it was found that the dissipated energy increased significantly in the presence of Ca ions. This hints at the presence of an ion-mediated organic network acting as a glue between the mineralised fibrils.[78] This concept is in line with the findings of Gupta *et al.*[71–73] and the importance of charge interactions[75] in the extrafibrillar space.

Although these experiments gave great insight into the deformation mechanisms in bone, the mechanical tests were performed mostly on specimens on the length scale of hundreds of micrometers to millimetres. Therefore, the measured response included the averaged deformation of a large number of osteons and no quantitative data was extracted about the local micromechanical strength properties on the length scale of a lamella.

For mineralised collagen fibrils, molecular dynamics simulations shed some light on their deformation and failure mechanisms.[79,80] By atomistic and coarse grained molecular dynamics simulations, it was found that the presence of mineral crystals provides additional resistance against plastic deformation and increases the fracture strength. The adhesion forces between the mineral platelets and collagen molecules remain weak allowing slippage following overloading, which serves as stress shielding against collagen fracture. This is in agreement with the hypothesis by Fritsch *et al.*[81] that bone failure involves slippage of mineral platelets lubricated by the presence of water followed by rupture of collagen. Gupta *et al.*[82] found during *in situ* diffraction experiments on tensile specimens of antler bone both interfibrillar deformation in the extrafibrillar space as well as intrafibrillar deformation at the collagen-mineral interface, which is in line with the findings of Buehler[79] and Nair *et al.*[80] Mechanical tests of single mineralised collagen fibrils[83] showed a wide range of strengths (40-490 MPa), but were in qualitative agreement with the simulations.

One of the most widely used micromechanical testing methods in bone is microindentation.[84,85] In this technique a diamond tip with known geometry is pressed into a flat sample surface and the force and tip displacement are recorded simultaneously. The pioneering work of Oliver and Pharr[86] allows the extraction of elastic properties from the unloading part of the indentation curve, while hardness or mean indentation pressure is related to the tested material's strength.[87] However, the determination of strength properties from microindentation data is complicated by the multiaxial and heterogeneous stress state under the indenter tip and bone's complex mechanical behaviour and necessitates the use of inverse methods based on finite element modelling.[45,88–90]

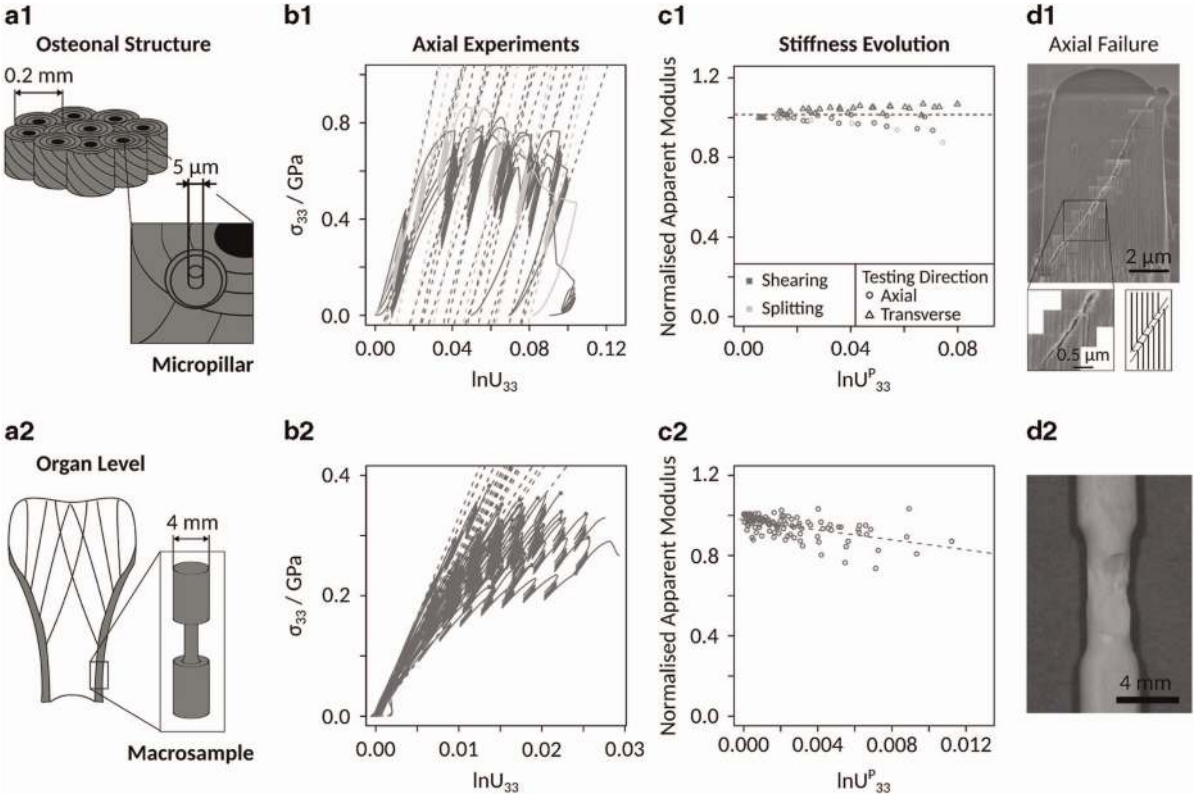

Figure 5 Scale transition of the mechanical behaviour shown by compression of micropillars on the lamellar level (1) and macroscopic dumbbell-shaped specimens (2).[40] (**a**) Sketch of the tested specimen size and shape compared to the relevant structural level of bone. (**b**) Stress-strain curves from uniaxial compression tests with partial unloading cycles to measure unloading modulus as a function of plastic strain showing a superior strength on the lamellar level. (**c**) Evolution of normalised apparent unloading modulus as a function of plastic strain showing an increased ductility and absence of damage on the lamellar level. (**d**) Images of the relevant failure mode showing a scale transition from homogeneous deformation followed by a single shear crack on the lamellar level to microcracking followed by catastrophic failure on the macroscale.

Tai *et al.*[88] performed a combination of microindentation with two different tips and finite element modelling using a cohesive-frictional Mohr-Coulomb yield criterion. They interpreted their findings by suggesting that nanogranular friction between mineral platelets is responsible for the tension-compression asymmetry in yield properties, while cohesion is originated by the organic matrix rather than organic-mineral bonding. They reported back-calculated strength values, which are similar to macroscopic properties as well as results from other microindentation based studies.[45,89,90] However, the inherent nanoporosity in the tissue[91] and the fact that bone does not exhibit pile-up behaviour around the indentation[58,88,89] would suggest the presence of plastic compressibility,[9] which was not accounted for in these studies.[92] Therefore, the strength values reported in such studies depend greatly on the assumptions about the material's plastic response rendering the generalisation of such results to other load cases very difficult.

It is not trivial to interpret microindentation data quantitatively in terms of strength, as indentations in materials with very different behaviours can result in very similar curves.[93] However, correlations of hardness with microstructural and compositional features can give an important insight into the mechanisms and relevant factors determining bone strength at the microscale. Correlation of hardness or modulus with microstructural properties like mineral fraction or collagen orientation showed good correlations in an interspecies study[94] and significant differences between osteonal bone and the more highly mineralised interstitial areas in human bone.[84,85] However, studies concentrating on human bone reported either low correlation coefficients[37,95,96] or even a lack of correlation[35,97,98] highlighting the importance of other factors like nanoporosity[98] or collagen cross-linking[37] and the relative inter-donor homogeneity of bone tissue on the lamellar level,[35] especially in the elderly. The intra-donor variation in indentation properties between osteonal and interstitial bone remains significant also in this age group.[35] Finally, it was hypothesised based on AFM-nanoindentation, reference point indentation, and macroscopic fracture tests, that nano- and micro-heterogeneity of local material properties could act as a toughening and strengthening mechanisms by redistributing stresses and deflecting crack paths.[99]

Recently, an alternative testing method has emerged, in which micron-sized micropillars milled by focused ion beam from a bulk sample are tested using a flat punch indenter.[100] The mostly homogeneous and uniaxial stress state inside the probed pillar[101] allows for a relatively straightforward interpretation of the data in terms of stress–strain relationships. This opens up the opportunity to measure yield and post-yield properties at the microscale in a quantitative fashion, which has been recently performed in dry condition on bone.[40,102] The experiments showed an anisotropic elastoplastic behaviour[40] with a superior strength of bone at the lamellar level (**Table 2**) and an increased ductility with strains up to 10–15% followed by failure in a single shear crack[40] (**Figure 5**).

This ductile behaviour of the quasi-brittle material bone is in line with the scaling theory of quasi-brittle failure[103] and may be explained by the fact that the size of the micropillar is smaller than the plastic process zone, which has been reported to be in the range of 20 μm.[104] The failure stress probability distribution function in this case follows a Gaussian and plastic behaviour dominates,[103] while microcracks do not develop easily in this situation. These experiments highlighted the presence of a size effect also in the hierarchical material bone (**Figure 5**) and the importance of interfaces and flaws such as cement interfaces, porosity and pre-existing cracks for the change in behaviour when testing larger specimens.[40] Recent microcantilever bending tests on rat bone[105] reported strength values in a similar range to Schwiedrzik *et al.*[40] However, the observed failure mode was brittle. This could hint at a loading mode dependent nanoscale deformation mechanism and plastic zone size, but further research in this area is needed.

Finally, all studies measuring microscale strength based on FIB-machined microspecimens so far[40,102,105] were performed in dry condition (in air or *in vacuo*). However, it has been shown in several microindentation studies that the hydration state has a severe impact on the micromechanical properties of bone.[40,70,106] Therefore, there is a clear need for further development toward testing of micron-sized cantilevers or pillars in hydrated conditions in order to measure physiologically relevant microscale strength properties.

Ageing and Disease

The following section is a brief introduction on the influence of ageing and different diseases on the post-yield mechanical properties of bone.

Osteoporosis is characterised by a loss of bone mass that induces a loss of structural integrity and it has been shown that porosity[32] increases significantly with donor age. More and smaller osteons are developed[31] over the live span but may reach asymptotic values in mature bone.[35] This changing heterogeneity decrease bone's overall strength and its toughness.[13,32,107,108] Although an increased cortical porosity in type 2 diabetic postmenopausal women with fragility fractures was found,[109] porosity, number of osteons, and osteonal diameter were gender independent in elderly cohorts of other studies.[35] In terms of bone quality, it could be shown that while composition and micromechanical properties of bone on the length scale of a lamella measured by Raman spectroscopy and microindentation change up to a certain age, they reach a plateau and remain mostly constant in the elderly.[35,85,70,96,110–112] It was found that the collagen network and the tissue water content may change with age which affects the mechanical properties.[69,113–115]

Microdamage increases exponentially with age,[42,116] while the ability to remodel bone and, thus, repair induced damage is impaired.[117,118] Cement line density was also found to increase with donor age.[35,108] Since shear motion is possible in these interfaces,[64] they are presumably the loci for emerging cracks. The age related differences in post-yield behaviour have been associated with this exponential increase[119] and it seems to play a decisive role in the variability of the post-yield behaviour in elderly donors.[35]

Hardness tests and electron probe microanalysis[97] in normal, osteoporotic and osteoarthritic bone from patients obtained during a total hip arthoplasty or hemi-arthoplasty following a femoral neck fracture showed a 7% decrease in microhardness for osteoarthritic patients, which may be attributed to an increased remodelling activity in osteoarthritic patients and thus a reduction in mean tissue age. Surprisingly, no differences were found in terms of composition between osteoarthritis and osteoporosis patients or male and female donors. However, this may be an artefact of the measurement technique, as electron microprobe analysis is not an ideal tool for measuring bone composition in a quantitative fashion.[97] In a recent study, no significant changes of micromechanical properties in the femoral diaphysis measured by microindentation were observed between patients suffering from osteopenia or osteoporosis and those who did not (classification based on hip areal bone mineral density).[35]

In other diseases, such as Paget's disease, high bone turnover and bone enlargement lead to localised deformities.[120] The high turnover alters the structural organisation of the tissue into a less organised patchwork of lamellar and woven bone[121] which may increase the heterogeneity of the post-yield properties and leads to a lower stiffness and higher ductility.[122] This effect may also be encountered in osteomalacia where a vitamin D deficiency leads to a significant undermineralisation of the tissue.[123]

Using molecular dynamics simulations, three major changes influencing the nano- and micromechanical mechanical properties due to osteogenesis imperfecta mutations could be identified.[124] These are a reduction of tropocollagen stiffness, decreased intermolecular adhesion and increased intermolecular spacing (and thus decreased cross-link density), and the formation of stress concentrations leading to a reduction of strength of the collagen fibril. Recent indentation studies reported a decrease in stiffness despite an increased mineralisation[125] and could verify the trend that stiffness reduces with increased disease severity.[126]

Conclusion

The reviewed data indicates that the post-yield behaviour of cortical bone has been well understood on the organ level (**Figure 2**). The underlying post-yield behaviour at the ECM level has yet to be unravelled. While first steps have been taken, especially the tension-compression asymmetry and the nature of the dissipation mechanism as well as the micromechanical strength properties under physiologic and diseased conditions are yet to be determined. Such knowledge could inform the development and realisation of tailored treatment strategies ranging from diagnostics to patient specific implant solution.

Conflict of Interest

The authors declare no conflict of interest.

References

1. Eswaran SK, Gupta A, Adams MF, Keaveny TM. Cortical and trabecular load sharing in the human vertebral body. *J Bone Miner Res* 2006; **21**: 307–314.
2. Holzer G, von Skrbensky G, Holzer LA, Pichl W. Hip fractures and the contribution of cortical versus trabecular bone to femoral neck strength. *J Bone Miner Res* 2009; **24**: 468–474.
3. Schaffler MB, Burr DB. Primate cortical bone microstructure: relationship to locomotion. *Am J Phys Anthropol* 1984; **65**: 191–197.
4. Treece GM, Gee AH, Mayhew PM, Poole KE. High resolution cortical bone thickness measurement from clinical CT data. *Med Image Anal* 2010; **14**: 276–290.

5. Zebaze RM, Ghasem-Zadeh A, Bohte A, Iuliano-Burns S, Mirams M, Price RI *et al.* Intracortical remodelling and porosity in the distal radius and post-mortem femurs of women: a cross-sectional study. *Lancet* 2010; **375**: 1672–1673.
6. Seeman E, Delmas PD. Bone quality – the material and structural basis of bone strength and fragility. *N Engl J Med* 2006; **354**: 2250–2261.
7. Cooper DML, Thomas CDL, Clement JG, Turinsky AL, Sensen CW, Hallgrimsson B. Age-dependent change in the 3D structure of cortical porosity at the human femoral midshaft. *Bone* 2007; **40**: 957–965.
8. Lemaitre J, Chaboche J-L. *Mechanics of Solid Materials*. Cambridge University Press, 2000.
9. Schwiedrzik JJ, Wolfram U, Zysset PK. A generalized anisotropic quadric yield criterion and its application to bone tissue at multiple length scales. *Biomech Model Mechanobiol* 2013; **12**: 1155–1168.
10. Wolfram U, Gross T, Pahr D, Schwiedrzik JJ, Wilke H-J, Zysset PK. Fabric based tsai-wu yield criteria for vertebral trabecular bone in stress and strain space. *J Mech Behav Biomed* 2012; **15**: 218–228.
11. Mirzaali M, Bürki A, Schwiedrzik JJ, Zysset PK, Wolfram U. Continuum damage interactions between tension and compression in osteonal bone. *J Mech Behav Biomed* 2015; **49**: 355–369.
12. Lemaitre J, Desmorat R. *Engineering Damage Mechanics – Ductile, Creep, Fatigue and Brittle Failures*. Springer: Berlin; Heidelberg; New York, 2005.
13. Currey JD. *Bones: Structure and Mechanics*. Princeton University Press, 2002.
14. Ritchie RO, Kinney JH, Kruzic JJ, Nalla RK. A fracture mechanics and mechanistic approach to the failure of cortical bone. *Fatigue Fract Eng Mater Struct* 2005; **28**: 345–371.
15. Zimmermann EA, Busse B, Ritchie RO. The fracture mechanics of human bone: Influence of disease and treatment. *BoneKey Rep* 2015; **4**: 1–13.
16. Rho JY, Kuhn-Spearing L, Zioupos P. Mechanical properties and the hierarchical structure of bone. *Med Eng Phys* 1998; **20**: 92–102.
17. Olszta MJ, Cheng X, Jee SS, Kumar R, Kim Y-Y, Kaufman MJ *et al.* Bone structure and formation: a new perspective. *Mater Sci Eng R* 2007; **58**: 77–116.
18. Nudelman F, Pieterse K, George A, Bomans PHH, Friedrich H, Brylka LJ *et al.* The role of collagen in bone apatite formation in the presence of hydroxyapatite nucleation inhibitors. *Nat Mater* 2010; **9**: 1004–1009.
19. Mahamid J, Addadi L, Weiner S. Chrystalization pathways in bone. *Cell Tissue Organ* 2011; **194**: 92–97.
20. Poundarik AA, Diab T, Sroga GE, Ural A, Boskey AL, Gundberg CM. Dilatational band formation in bone. *Proc Natl Acad Sci USA* 2012; **109**: 19178–19183.
21. Weiner S, Arad T, Sabanay I, Traub W. Rotated plywood structure of primary lamellar bone in the rat: orientations of the collagen fibril arrays. *Bone* 1997; **20**: 6.
22. Varga P, Pacureanu A, Langer M, Suhonen H, Hesse B, Grimal Q *et al.* Investigation of the 3D orientation of mineralized collagen fibrils in human lamellar bone using synchrotron X-ray phase nano-tomography. *Acta Biomater* 2013; **9**: 8118–8127.
23. Martin RB. Porosity and specific surface of bone. *Crit Rev Biomed Eng* 1984; **10**: 179–222.
24. Fratzl P, Weinkamer R. Nature's hierarchical materials. *Prog Mater Sci* 2007; **52**: 1263–1334.
25. Burr DB, Schaffler MB, Frederickson RG. Composition of the cement line and its possible mechanical role as a local interface in human compact bone. *J Biomech* 1988; **21**: 939–945.
26. Schaffler MB, Burr DB, Frederickson RG. Morphology of the osteonal cement line in human bone. *Anat Rec* 1987; **217**: 223–228.
27. Jepsen KJ, Davy DT, Krzypow DJ. The role of the lamellar interface during torsional yielding of human cortical bone. *J Biomech* 1999; **32**: 303–310.
28. Yeni YN, Norman TL. Calculation of porosity and osteonal cement line effects on the effective fracture toughness of cortical bone in longitudinal crack growth. *J Biomed Mater Res* 2000; **51**: 504–509.
29. Ebacher V, Wang R. A unique microcracking process associated with the inelastic deformation in haversian bone. *Adv Funct Mater* 2009; **19**: 57–66.
30. Nobakhti S, Limbert G, Thurner PJ. Cement lines and interlamellar areas in compact bone as strain amplifiers–Contributors to elasticity, fracture toughness and mechanotransduction. *J Mech Behav Biomed* 2014; **29**: 235–251.
31. Evans FG. Mechanical properties and histology of cortical bone from younger and older men. *Anat Rec* 1976; **185**: 1–12.
32. McCalden RW, McGeough JA, Barker MB, Court-Brown CM. Age-related changes in the tensile properties of cortical bone. The relative importance of changes in porosity, mineralization, and microstructure. *J Bone Joint Surg Am* 1993; **75**: 1193–1205.
33. Bayraktar HH, Morgan EF, Niebur GL, Morris GE, Wong EK, Keaveny TM. Comparison of the elastic and yield properties of human femoral trabecular and cortical bone tissue. *J Biomech* 2004; **37**: 27–35.
34. Doblar M, Garc JM, Gomez MJ. Modelling bone tissue fracture and healing: a review. *Eng Fract Mech* 2004; **71**: 1809–1840.
35. Mirzaali MJ, Schwiedrzik JJ, Thaiwichai S, Best JP, Michler J, Zysset PK *et al.* Mechanical properties of cortical bone and their relationships with age, gender, composition and microindentation properties in the elderly. *Bone* 2015; pii: S8756-3282(15)00419-6.
36. Martin RB, Ishida J. The relative effects of collagen fiber orientation, porosity, density, and mineralization on bone strength. *J Biomech* 1989; **22**: 419–426.
37. Bala Y, Depalle B, Douillard T, Meille S, Clément P, Follet H *et al.* Respective roles of organic and mineral components of human cortical bone matrix in micromechanical behavior: an instrumented indentation study. *J Mech Behav Biomed* 2011; **4**: 1473–1482.
38. Garnero P. The contribution of collagen crosslinks to bone strength. *BoneKey Rep* 2012; **1**: 1–8.
39. Schwiedrzik J, Gross T, Bina M, Pretterklieber M, Zysset P, Pahr D. Experimental validation of a nonlinear μFE model based on cohesive-frictional plasticity for trabecular bone. *Int J Numer Method Biomed Eng* 2016; **32**: e02739.
40. Schwiedrzik JJ, Raghavan R, Bürki A, LeNader V, Wolfram U, Michler J *et al. In situ* micropillar compression reveals superior strength and ductility but an absence of damage in lamellar bone. *Nat Mater* 2014; **13**: 740–747.
41. Schaffler MB, Radin EL, Burr DB. Mechanical and morphological effects of strain rate on fatigue of compact bone. *Bone* 1989; **10**: 207–214.
42. Burr DB, Forwood MR, Fyhrie DP, Martin RB, Schaffler MB, Turner CH. Bone microdamage and skeletal fragility in osteoporotic and stress fractures. *J Bone Miner Res* 1997; **12**: 6–15.
43. Vashishth D. Hierarchiy of bone microdamage at multiple length scales. *Int J Fatigue* 2007; **29**: 1024–1033.
44. Reilly GC, Currey JD. The development of microcracking and failure in bone depends on the loading mode to which it is adapted. *J Exp Biol* 1999; **20**: 543–552.
45. Zhang J, Michalenko MM, Kuhl E, Ovaert TC. Characterization of indentation response and stiffness reduction of bone using a continuum damage model. *J Mech Behav Biomed* 2010; **3**: 189–202.
46. O'Brien FJ, Taylor D, Dickson GR, Lee CT. Visualisation of three-dimensional microcracks in compact bone. *J Anat* 2000; **197**: 413–420.
47. O'Brien FJ, Taylor D, Lee TC. The effect of bone microstructure on the initiation and growth of microcracks. *J Orthop Res* 2005; **23**: 475–480.
48. O'Brien FJ, Taylor D, Lee TC. Bone as a composite material: The role of osteons as barriers to crack growth in compact bone. *Int J Fatigue* 2007; **29**: 1051–1056.
49. Ebacher V, Guy P, Oxland TR, Wang R. Sub-lamellar microcracking and roles of canaliculi in human cortical bone. *Acta Biomater* 2012; **8**: 1093–1100.
50. Jepsen KJ, Davy DT. Comparison of damage accumulation measures in human cortical bone. *J Biomech* 1997; **30**: 891–894.
51. Boyce TM, Fyhrie DP, Glotkowski MC, Radin EL, Schaffler MB. Damage type and strain mode associations in human compact bone bending fatigue. *J Orthop Res* 1998; **16**: 322–329.
52. Diab T, Vashishth D. Effects of damage morphology on cortical bone fragility. *Bone* 2005; **37**: 96–102.
53. Reilly DT, Burstein AH. The elastic and ultimate properties of compact bone tissue. *J Biomech* 1975; **8**: 393–405.
54. Caler WE, Carter DR. Bone creep-fatigue damage accumulation. *J Biomech* 1989; **22**: 625–635.
55. Reilly DT, Burstein AH, Frankel VH. The elastic modulus for bone. *J Biomech* 1974; **7**: 271–275.
56. Nyman JS, Leng H, Dong X, Wang XN. Differences in the mechanical behavior of cortical bone between compression and tension when subjected to progressive loading. *J Mech Behav Biomed* 2009; **2**: 613–619.
57. Li S, Demirci E, Silberschmidt VV. Variability and anisotropy of mechanical behavior of cortical bone in tension and compression. *J Mech Behav Biomed* 2013; **21**: 109–120.
58. Schwiedrzik JJ, Zysset PK. Quantitative analysis of imprint shape and its relation to mechanical properties measured by microindentation in bone. *J Biomech* 2015; **48**: 210–216.
59. Sun X, Hoon Jeon J, Blendell J, Akkus O. Visualization of a phantom post-yield deformation process in cortical bone. *J Biomech* 2010; **43**: 1989–1996.
60. Cezayirlioglu H, Bahniuk E, Davy DT, Heiple KG. Anisotropic yield behavior of bone under combined axial force and torque. *J Biomech* 1985; **18**: 61–69.
61. Turner CH, Wang T, Burr DB. Shear strength and fatigue properties of human cortical bone determined from pure shear tests. *Calcified Tiss Int* 2001; **69**: 373–378.
62. Dong XN, Acuna RL, Luo Q, Wang X. Orientation dependence of progressive post-yield behavior of human cortical bone in compression. *J Biomech* 2012; **45**: 2829–2834.
63. Tang T, Ebacher V, Cripton P, Guy P, McKay H, Wang R. Shear deformation and fracture of human cortical bone. *Bone* 2015; **71**: 25–35.
64. Lakes R, Saha S. Cement line motion in bone. *Science* 1979; **204**: 501–503.
65. Fondrk M, Bahniuk E, Davy DT, Michaels C. Some viscoplastic characteristics of bovine and human cortical bone. *J Biomech* 1988; **21**: 623–630.
66. Hansen U, Zioupos P, Simpson R, Currey JD, Hynd D. The effect of strain rate on the mechanical properties of human cortical bone. *J Biomech Eng* 2008; **130**: 011011.
67. Zioupos P, Hansen U, Currey JD. Microcracking damage and the fracture process in relation to strain rate in human cortical bone tensile failure. *J Biomech* 2008; **41**: 2932–2939.
68. Johnson TPM, Socrate S, Boyce MC. A viscoelastic, viscoplastic model of cortical bone valid at low and high strain rates. *Acta Biomater* 2010; **6**: 4073–4080.
69. Nyman JS, Roy A, Shen X, Acuna RL, Tyler JH, Wang X. The influence of water removal on the strength and toughness of cortical bone. *J Biomech* 2006; **39**: 931–938.
70. Wolfram U, Wilke H-J, Zysset PK. Rehydration of vertebral trabecular bone: influences on its anisotropy, its stiffness and the indentation work with a view to age, gender and vertebral level. *Bone* 2010; **46**: 348–354.
71. Gupta HS, Seto J, Wagermaier W, Zaslansky P, Boesecke P, Fratzl P. Cooperative deformation of mineral and collagen in bone at the nanoscale. *Proc Natl Acad Sci USA* 2006; **103**: 17741–17746.
72. Gupta HS, Wagermaier W, Zickler GA, Raz-Ben AD, Funari SS, Roschger P *et al.* Nanoscale deformation mechanisms in bone. *Nano Lett* 2005; **5**: 2108–2111.
73. Gupta HS, Wagermaier W, Zickler GA, Hartmann J, Funari SS, Roschger P. Fibrillar level fracture in bone beyond the yield point. *Int J Fract* 2006; **139**: 425–436.
74. Schoeck G. The activation energy of dislocation movement. *Physica Status Solidi B* 1965; **8**: 499–507.

75. Gupta HS, Fratzl P, Kerschnitzki M, Benecke G, Wagermaier W, Kirchner HO. Evidence for an elementary process in bone plasticity with an activation enthalpy of 1 eV. *J R Soc Interface* 2007; **4**: 277–282.
76. Fantner T, Hassenkam GE, Kindt JH, Weaver JC, Birkedal H, Pechenik L, Cutroni JA *et al.* Sacrificial bonds and hidden length dissipate energy as mineralized fibrils separate during bone fracture. *Nat Mater* 2005; **4**: 612–616.
77. Fantner GE, Rabinovych O, Schitter G, Thurner P, Kindt JH, Finch MM *et al.* Hierarchical interconnections in the nano-composite material bone: Fibrillar cross-links resist fracture on several length scales. *Compos Sci Technol* 2006; **66**: 1205–1211.
78. Fantner GE, Adams J, Turner P, Thurner PJ, Fisher LW, Hansma PK. Nanoscale ion mediated networks in bone: osteopontin can repeatedly dissipate large amounts of energy. *Nano Lett* 2007; **7**: 2491–2498.
79. Buehler MJ. Molecular nanomechanics of nascent bone: fibrillar toughening by mineralization. *Nanotechnol* 2007; **18**: 295102.
80. Nair AK, Gautieri A, Chang S-W, Buehler MJ. Molecular mechanics of mineralized collagen fibrils in bone. *Nat Commun* 2013; **4**: 1724.
81. Fritsch A, Hellmich C, Dormieux L. Ductile sliding between mineral crystals followed by rupture of collagen crosslinks: Experimentally supported micromechanical explanation of bone strength. *J Theor Biol* 2009; **260**: 230–252.
82. Gupta HS, Krauss S, Kerschnitzki M, Karunaratne A, Dunlop JWC, Barber AH *et al.* Intrafibrillar plasticity through mineral/collagen sliding is the dominant mechanism for the extreme toughness of antler bone. *J Mech Behav Biomed* 2013; **28**: 366–382.
83. Shen ZL, Dodge MR, Kahn H, Ballarini R, Eppell SJ. *In vitro* fracture testing of submicron diameter collagen fibril specimens. *Biophys J* 2010; **99**: 1986–1995.
84. Rho J-Y, Tsui TY, Pharr GM. Elastic properties of human cortical and trabecular lamellar bone measured by nanoindentation. *Biomaterials* 1997; **20**: 1325–1330.
85. Zysset PK, Guo EX, Hoffler EC, Moore KE, Goldstein SA. Elastic modulus and hardness of cortical and trabecular bone lamellae measured by nanoindentation in the human femur. *J Biomech* 1999; **32**: 1005–1012.
86. Oliver WC, Pharr GM. An improved technique for determining hardness and elastic modulus using load and displacement sensing indentation experiments. *J Mater Res* 1992; **7**: 1564–1583.
87. Anthony C. Fischer-Cripps. *Nanoindentation*. Springer-Verlag: New York, NY, USA, 2002.
88. Tai K, Ulm F-J, Ortiz C. Nanogranular origins of the strength of bone. *Nano Lett* 2006; **6**: 2520–2525.
89. Mullins LP, Bruzzi MS, McHugh PE. Calibration of a constitutive model for the post-yield behaviour of cortical bone. *J Mech Behav Biomed* 2009; **2**: 460–470.
90. Lucchini R, Carnelli D, Ponzoni M, Bertarelli E, Gastaldi D, Vena P. Role of damage mechanics in nanoindentation of lamellar bone at multiple sizes: experiments and numerical modeling. *J Mech Behav Biomed* 2011; **4**: 1852–1863.
91. Nielsen-Marsh CM, Hedges REM. Bone porosity and the use of mercury intrusion porosimetry in bone diagenesis studies. *Archaeometry* 1999; **41**: 165–174.
92. Schwiedrzik JJ, Zysset PK. The influence of yield surface shape and damage in the depth-dependent response of bone tissue to nanoindentation using spherical and Berkovich indenters. *Comput Method Biomech* 2015; **18**: 492–505.
93. Chen X, Ogasawara N, Zhao M, Chiba N. On the uniqueness of measuring elastoplastic properties from indentation: The indistinguishable mystical materials. *J Mech Phys Solids* 2007; **55**: 1618–1660.
94. Hodgskinson R, Currey JD, Evans GP. Hardness, an indicator of the mechanical competence of cancellous bone. *J Orthop Res* 1989; **7**: 754–758.
95. Hengsberger S, Boivin G, Zysset PK. Morphological and mechanical properties of bone structural units: a two-case study. *JSME Int J C* 2002; **45**: 936–943.
96. Boivin G, Bala Y, Doublier A, Farlay D, Ste-Marie LG, Meunier PJ *et al.* The role of mineralization and organic matrix in the microhardness of bone tissue from controls and osteoporotic patients. *Bone* 2008; **43**: 532–538.
97. Coats A, Zioupos P, Aspden R. Material properties of subchondral bone from patients with osteoporosis or osteoarthritis by microindentation testing and electron probe microanalysis. *Calcif Tissue Int* 2003; **73**: 66–71.
98. Spiesz EM, Reisinger AG, Kaminsky W, Roschger P, Pahr DH, Zysset PK. Computational and experimental methodology for site-matched investigations of the influence of mineral mass fraction and collagen orientation on the axial indentation modulus of lamellar bone. *J Mech Behav Biomed* 2013; **28**: 195–205.
99. Katsamenis OL, Jenkins T, Thurner PJ. Toughness and damage susceptibility in human cortical bone is proportional to mechanical inhomogeneity at the osteonal-level. *Bone* 2015; **76**: 158–168.
100. Uchic MD, Dimiduk DM. A methodology to investigate size scale effects in crystalline plasticity using uniaxial compression testing. *Mater Sci Eng A* 2005; **400**: 268–278.
101. Maeder X, Mook WM, Niederberger C, Michler J. Quantitative stress/strain mapping during micropillar compression. *Philos Mag* 2011; **91**: 1097–1107.
102. Luczynski KW, Steiger-Thirsfeld A, Bernardi J, Eberhardsteiner J, Hellmich C. Extracellular bone matrix exhibits hardening elastoplasticity and more than double cortical strength: Evidence from homogeneous compression of non-tapered single micron-sized pillars welded to a rigid substrate. *J Mech Behav Biomed* 2015; **52**: 51–62.
103. Bažant ZP. Scaling theory for quasibrittle structural failure. *Proc Natl Acad Sci USA* 2004; **101**: 13400–13407.
104. Robertson DM, Robertson D, Barrett CR. Fracture toughness, critical crack length and plastic zone size in bone. *J Biomech* 1978; **11**: 359–364.
105. Jimenez-Palomar I, Shipov A, Shahar R, Barber AH. Structural orientation dependent sub-lamellar bone mechanics. *J Mech Behav Biomed* 2015; **52**: 63–71.
106. Rodriguez-Florez N, Oyen ML, Shefelbine SJ. Insight into differences in nanoindentation properties of bone. *J Mech Behav Biomed* 2013; **18**: 90–99.
107. Zioupos P, Kaffy C, Currey JD. Tissue heterogeneity, composite architecture and fractal dimension effects in the fracture of ageing human bone. *Int J Fract* 2006; **139**: 407–424.
108. Zimmermann EA, Schaible E, Bale H, Barth HD, Tang SY, Reichert P *et al.* Age-related changes in the plasticity and toughness of human cortical bone at multiple length scales. *Proc Natl Acad Sci USA* 2011; **108**: 14416–14421.
109. Patsch JM, Burghardt AJ, Yap SP, Baum T, Schwartz AV, Joseph GB *et al.* Increased cortical porosity in type 2 diabetic postmenopausal women with fragility fractures. *J Bone Miner Res* 2013; **28**: 313–324.
110. Gamsjaeger S, Buchinger B, Zwettler E, Recker R, Black D, Gasser JA *et al.* Bone material properties in actively bone-forming trabeculae in postmenopausal women with osteoporosis after three years of treatment with once-yearly Zoledronic acid. *J Bone Miner Res* 2011; **26**: 12–18.
111. Paschalis EP, Fratzl P, Gamsjaeger S, Hassler N, Brozek W, Eriksen EF *et al.* Aging versus postmenopausal osteoporosis: bone composition and maturation kinetics at actively-forming trabecular surfaces of female subjects aged 1 to 84 years. *J Bone Miner Res* 2015; **31**: 347–357.
112. Thurner PJ. Commentary on: mechanical properties of cortical bone and their relationships with age, gender, composition and microindentation properties in the elderly. *Bone* 2016; **87**: 159.
113. Viguet-Carrin S, Garnero P, Delmas PD. The role of collagen in bone strength. *Osteoporos Int* 2006; **17**: 319–336.
114. Unal M, Yang S, Akkus O. Molecular spectroscopic identification of the water compartments in bone. *Bone* 2014; **67**: 228–236.
115. Granke M, Does MD, Nyman JS. The role of water compartments in the material properties of cortical bone. *Calcif Tissue Int* 2015; **97**: 292–307.
116. Schaffler MB, Choi K, Milgrom C. Aging and matrix microdamage accumulation in human compact bone. *Bone* 1995; **17**: 521–525.
117. Sambrook P, Cooper C. Osteoporosis. *Lancet* 2006; **367**: 2010–2018.
118. Teti A. Bone Development: Overview of bone cells and signalling. *Curr Osteoporos Rep* 2011; **9**: 264–273.
119. Courtney AC, Hayes WC, Gibson LJ. Age-related differences in post-yield damage in human cortical bone. Experiment and model. *J Biomech* 1996; **29**: 1463–1471.
120. Seitz S, Priemel M, Zustin J, Beil FT, Semler J, Minne H *et al.* Paget's disease of bone: histologic analysis of 754 patients. *J Bone Miner Res* 2009; **24**: 62–69.
121. Meunier PJ, Coindre JM, Edouard CM, Arlot ME. Bone histomorphometry in Paget's disease quantitative and dynamic analysis of pagetic and nonpagetic bone tissue. *Arthritis Rheum* 1980; **23**: 1095–1103.
122. Zimmermann EA, Köhne T, Bale HA, Panganiban B, Gludovatz B, Zustin J *et al.* Modifications to nano- and microstructural quality and the effects on mechanical Integrity in paget's disease of bone. *J Bone Miner Res* 2015; **30**: 264–273.
123. Whyte MP, Thakker RV. Rickets and osteomalacia. *Medicine (Baltimore)* 2005; **33**: 70–74.
124. Gautieri A, Uzel S, Vesentini S, Redaelli A, Buehler MJ. Molecular and mesoscale mechanisms of osteogenesis imperfecta disease in collagen fibrils. *Biophys J* 2009; **97**: 857–865issn: 0006-3495.
125. Vanleene M, Porter A, Guillot P-V, Boyde A, Oyen M, Shefelbine S. Ultrastructural defects cause low bone matrix stiffness despite high mineralization in osteogenesis imperfecta mice. *Bone* 2012; **50**: 1317–1323.
126. Albert C, Jameson J, Toth JM, Smith P, Harris G. Bone properties by nanoindentation in mild and severe osteogenesis imperfecta. *Clin Biomech* 2013; **28**: 110–116.
127. Carter DR, Caler WE, Spencler DM, Frankel VH. Fatigue behavior of adult cortical bone: The Influence of mean strain and strain range. *Acta Orthop* 1981; **52**: 481–490.
128. Currey JD. Tensile yield in compact bone is determined by strain, post-yield behaviour by mineral content. *J Biomech* 2004; **37**: 549–556.
129. Dickenson RP, Hutton WC, Stott JRR. The mechanical properties of bone in osteoporosis. *J Bone Joint Surg* 1981; **63**: 233–238.
130. Dong XN, Luo Q, Wang X. Progressive post-yield behavior of human cortical bone in shear. *Bone* 2013; **53**: 1–5.
131. Duchemin L, Bousson V, Raossanaly C, Bergot C, Laredo JD, Skalli W *et al.* Prediction of mechanical properties of cortical bone by quantitative computed tomography. *Med Eng Phys* 2008; **30**: 321–328.
132. Lee SC, Coan BS, Bouxsein ML. Tibial ultrasound velocity measured in situ predicts the material properties of tibial cortical bone. *Bone* 1997; **21**: 119–125.
133. Leng H, Dong XN, Wang X. Progressive post-yield behavior of human cortical bone in compression for middle-aged and elderly groups. *J Biomech* 2009; **42**: 491–497.
134. Nyman JS, Roy A, Reyes MJ, Wang X. Mechanical behavior of human cortical bone in cycles of advancing tensile strain for two age groups. *J Biomed Mater Res A* 2009; **89**: 521–529.
135. Saha S. Longitudinal shear properties of human compact bone and its constituents, and the associated failure mechanisms. *J Mater Res* 1977; **12**: 1798–1806.
136. Wang X, Nyman JS. A novel approach to assess post-yield energy dissipation of bone in tension. *J Biomech* 2007; **40**: 674–677.
137. Yamada H. *Strength of Biological Materials*. Evans FG (ed.). Williams & Wilkins Company: Baltimore, MD, USA, 1970.
138. Reisinger AG, Pahr DH, Zysset PK. Sensitivity analysis and parametric study of elastic properties of an unidirectional mineralized bone fibril-array using mean field methods. *Biomech Model Mechanobiol* 2010; **9**: 499–510.